Journal of Geology & Geophysics
ISSN: 2381-8719

Boori et al., J Geol Geophys 2015, 4:5
DOI: 10.4172/2381-8719.1000223

Research Article Open Access

Land Surface Temperature and Scaling Factors for Different Satellites Datasets

Mukesh Singh Boori[1,4]*, Heiko Balzter[3], Komal Choudhary[1] and Vit Vozenílek[4]

[1]Samara State Aerospace University, Russia
[2]American Sentinel University, Colorado, USA
[3]University of Leicester England, UK
[4]Palacky University Olomouc, Czech Republic

Abstract

Land surface parameters are highly integrated and have a direct effect on water and energy balance and weather predictions. Due to the difficulties in correcting the influences of the atmosphere absorbability and the earth surface emissivity diversification, the retrieval of land surface temperature (LST) from satellite data is a challenging task. To retrieve microwave land emissivity, infrared surface skin temperatures have been used as surface physical temperature. However, passive microwave emissions originate from deeper layers with respect to the skin temperature. So, this inconsistency in sensitivity depths between skin temperatures and microwave temperatures may introduce a discrepancy in the determined emissivity. In this research, six sample sites were chosen on the earth for 2013 and 2014 and then land surface temperature from AMSR-2, Landsat and ASTER brightness temperature values have been derived. The algorithm has been developed from a surface brightness temperature dataset, which has used as inputs surface parameters and atmospheric quantities. The retrieved LST has been compared within AMSR-2, Landsat and ASTER for the same period and area. Maximum time ASTER has shown higher temperature than other data and AMSR-2 has lower temperature on same area. Landsat and ASTER is closer to ground measured temperature than AMSR-2 data. It will be interesting to see how the satellite-derived surface temperature will behave in an assimilation scheme in a follow-up study.

Keywords: AMSR-2; ASTER; Landsat data; Brightness temperature

Introduction

Surface temperature is a key parameter in many energy balance applications, such as evaporation models, climate models and radiative transfer models. Land/use cover (in terms of temperature and soil moisture) affect the surrounding climate, such as the water vapours, the dust partials, the gas molecules and the clouds formation; so it directly affects rain and then land/use cover [1]. By this way, it affects the whole ecosystem and correlates with natural disasters. Land Surface Models (LSMs) are expected to lead to improved short-term to long-range forecasting models. Because the land/surface parameters are highly integrated, errors in land surface forcing, model physics and parameterization tend to accumulate in the land surface stores of these models, such as soil moisture and surface temperature [2-4]. This has a direct effect on the models' water and energy balance calculations, and may eventually result in inaccurate weather predictions. Timely monitoring of natural disasters is important for minimizing economic losses caused by floods, drought, etc. so it's important for emergency management during natural disasters. Consequently, remote sensing for land/surface temperature has become an important research subject to a global scale [5].

Ground observations are generally useful for local applications; however, they are highly intensive in man-power and equipment costs. Furthermore, ground observations of land surface temperature are point measurements and since variability can be high, especially in regions with discontinuous vegetation, scaling up to spatial averages is often difficult [6]. In other side satellite-generated brightness temperatures (BT) are more convenient on global level and temporal basis [7,8].

Instantaneous measures of microwave brightness temperature (BT) have been used in a variety of applications to estimate column water vapour abundance, rainfall rate, surface ocean wind speed, ocean salinity, soil moisture, freeze/thaw state, land surface temperature, inundation fraction, and vegetation structure [9-14]. Land surface properties can be inferred accurately if physical temperature and emissivity variations can be separated [15,16]. Diurnal synoptic and variations of land surface temperature, as well as the atmospheric temperature and water vapour profiles, affect the observed BT. More frequent are the observations of BT throughout the day, the better understanding of the variability of the retrieved parameters is obtained [17].

There are a very few studies dealing with the characterization of the BT diurnal variation over land. The diurnal variation of physical and brightness temperatures as a function of incident solar radiation has been modelled for the Tropical Rainfall Measuring Mission (TRMM) Microwave Imager (TMI) [18]. The characteristics of the skin temperature diurnal cycles as measured from IR over different land types were investigated. In densely vegetated areas with more moisture, skin temperature exhibits a smaller diurnal variation than in arid and desert areas [19].

The paper is organized in the sections below. Following the description of the study area in Section 2, brief discussion about

***Corresponding author:** Mukesh Singh Boori, Department of Geo-informatics, Section of Earth Sciences Palacký University, Czech Republic, Tel: +420585631111; E-mail: mukesh.boori@upol.cz

Received July 08, 2015; **Accepted** September 15, 2015; **Published** September 30, 2015

Citation: Boori MS, Balzter H, Choudhary K, Vozenílek V (2015) Land Surface Temperature and Scaling Factors for Different Satellites Datasets. J Geol Geophys 4: 223. doi:10.4172/2381-8719.1000223

datasets in section-3, the methodology of calculating LST, and a brief introduction to normalized mutual information measure are presented in Section 4. The analysis and conclusions are presented in Sections 5-6, respectively.

Study Area

The study area has six training sites on earth in different continent in order to compare the temperature in different satellite datasets in same location (Figure 1). Sample sites are located in the following places: (1) Karl Stefan Memorial Airport (USA); (2) Mondai, Santa Catarina (Brazil); (3) Belgrade, Serbia (Europe); (4) Khartoum, Sudan (Africa); (5) Chengdu, China; (6) Kalgoorlie, Australia.

Data Sets

This research work has used thermal bands of AMSR-2, Landsat and ASTER satellite data. Technical characteristics of used satellite data are listed as it follows:

AMSR2

The Advanced Microwave Scanning Radiometer-2 (AMSR-2) on board the GCOM-W1 satellite is a remote sensing instrument for measuring weak microwave emission from the surface and the atmosphere of the Earth. From about 700 km above the Earth, AMSR-2 provides highly accurate measurements of the intensity and scattering of microwave emissions and scattering. The antenna of AMSR-2 rotates once per 1.5 seconds and obtains data over a 1450 km swath. This conical scan mechanism enables AMSR-2 to acquire a set of daytime and night time data with more than 99% coverage of the earth every 2 days. It's had 7 frequencies with vertical and horizontal polarizations. Here 36.5 GHz vertical frequency was used for land surface temperature, get from Japan Aerospace Exploration Agency. The 36.5 GHz AMSR-2 footprint is an oval of 25 km square, where the derived surface temperature fields are resampled in a 0.25 degree grid. A subset covering the sample sites is cut from the global dataset. The choice for these location is motivated by the presence of sets of observational data for the corresponding period of time (i.e. year 2013-14) and there availability. Observed data is collected from 6 stations located on earth, spatially representative of different types of land cover [20] (Figure 1).

Landsat

In this research work Landsat 8 satellite data was used. Landsat 8 carries two instruments: The Operational Land Imager (OLI) sensor and Thermal Infrared Sensor (TIRS) sensor. The TIRS sensor provides two thermal bands. These sensors provide improved signal-to-noise (SNR) radiometric performance quantized over a 12-bit dynamic range. This translates into 4096 potential grey levels in an image compared with only 256 grey levels in previous 8-bit instruments. Improved signal-to-noise performance enables a better characterization of land cover state and condition [21]. This product is delivered as 16-bit images (scaled to 55,000 grey levels). For this research work band number 11TIRS (11.5-12.51 µm) 100 m was used for surface temperature.

ASTER

ASTER data provides the user community with standard data products throughout the life of the mission. Algorithms to compute these products were created by the ASTER science team, and are implemented at the Land Processes Distributed Active Archive Centre (LP DAAC). Users can search and browse these products through GDS and NASA Reverb. For this research work band number 14 TIR (10.95-11.65 µm) was used for surface temperature. It's have 16 bit data with +/-8.55 telescope pointing capacity [22].

Methodology

In our previous study, we estimated microwave land surface emissivity over the globe from AMSR-E observations at all frequencies and polarizations [23]. The previous emissivity retrieval

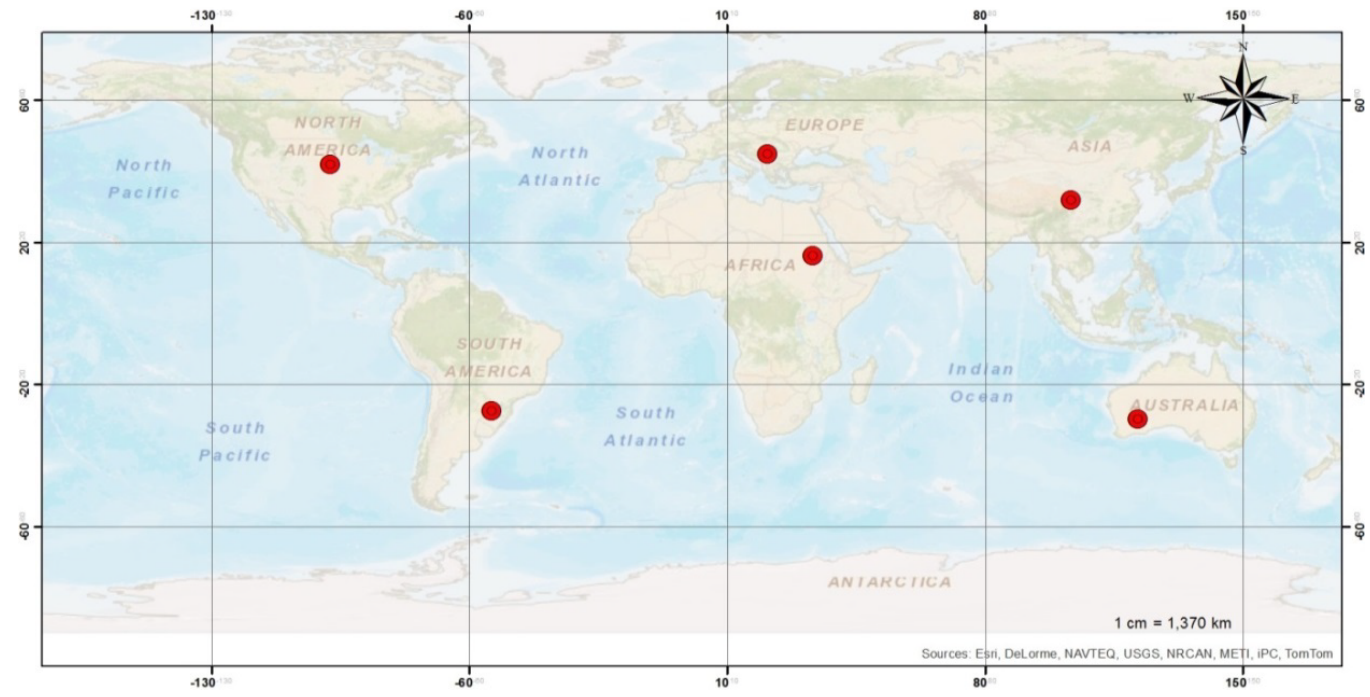

Figure 1: Observed data taken stations located on the Earth.

is based on the assumption that the infrared skin temperature is the effective physical temperature, which is equivalent to assume that the microwave brightness temperature originates from the skin. This assumption is not always true, but necessary due to the lacking of general globe information on penetration depths and temperature profiles.

A physical model was proposed to account for the effect of penetration depth on emissivity retrievals by revising the physical temperature [24]. In this research work, first take sample sites and then derive land surface temperature from satellite brightness temperature by the help of following scaling factors for different satellite data [25]:

AMSR-2

For AMSR2 data scale factor is set as 0.01 [K]. For instance, if brightness temperature data is stored as 28312, original value of the data is 283.12 [K].

ASTER

ASTER surface temperatures are computed from spectral radiance so begins by converting DNs to radiance and for that equation is following:

L_λ=(DN-1) X UCC

Where L_λ is the spectral radiance, DN are the TIR band digital numbers, and UCC are the published Unit Conversion Coefficients (0.005225 $w/m^{-2}/sr^{-1}/\mu m^{-1}$).

Temperature (measured in degrees Kelvin) is then given by:

$T=K2 / (\ln (K1/ L_\lambda+1)$

Where K1 (641.32) and K2 (1271.22) are constants derived from Planck's radiance function.

Landsat

OLI and TIRS band data can be converted to TOA spectral radiance using the radiance rescaling factors provided in the metadata file:

$L_\lambda = M_L Q_{cal} + A_L$

where:

L_λ=TOA spectral radiance ($w/m^{-2}/sr^{-1}/\mu m^{-1}$)

M_L=Band-specific multiplicative rescaling factor from the metadata

(RADIANCE_MULT_BAND_x, where x is the band number)

A_L=Band-specific additive rescaling factor from the metadata

(RADIANCE_ADD_BAND_x, where x is the band number)

Q_{cal}=Quantized and calibrated standard product pixel values (DN)

TIRS band data can be converted from spectral radiance to brightness temperature using the thermal constants provided in the metadata file:

$T=K2/(\ln (K1/L_\lambda+1)$

where:

T=At-satellite brightness temperature (K)

L_λ=TOA spectral radiance ($w/m^{-2}/sr^{-1}/\mu m^{-1}$)

K_1=Band-specific thermal conversion constant from the metadata

(K1_CONSTANT_BAND_x, where x is the band number, 10 or 11)

K_2=Band-specific thermal conversion constant from the metadata

(K2_CONSTANT_BAND_x, where x is the band number, 10 or 11)

Analysis Results

In the following section, 1° × 1° spatial subsets of the products were co-registered so that the resulting subsets cover the same area as the Landsat, ASTER and AMSR-2 images in Figures 2-4. Where necessary, spatial re-sampling was performed using the 'nearest neighbour' method. The gravel plains are highly homogenous in space and time and outside globe two seasons (around September and June) the chances for precipitation are remote therefore, it is safe to assume that the land surface was completely dry for the results presented in this paper. The following section briefly discusses the actual land surface temperature on the same area and time from different satellite datasets (Figures 2-4).

AMSR-2

Figure 2 shows an example of the AMSR-2 surface temperature retrievals at day time in June 2014 and September 2013, when observational data have been sampled.

AMSR-2 June 2014 data show minimum 166.67 K and highest 305.34 K temperature and for September 2013 minimum is 170.78 K and highest is 305.34 K temperature. In June highest temperature is present in Sahara desert, western centre of North America and north-eastern part of Brazil, western sector of India and China. In September 2013 is the same like 2014 but high temperature is also present in Australian desert, in reduced areas of India and China but increased areas of South Africa and South America (Figure 2).

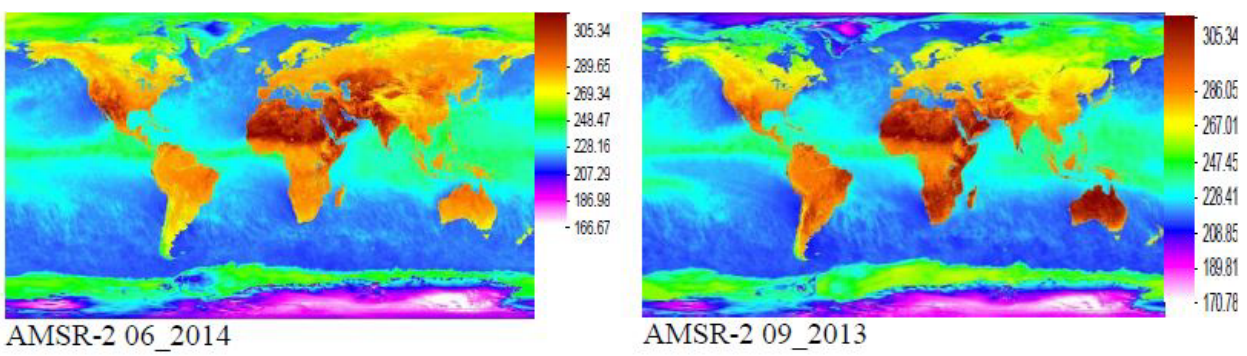

Figure 2: AMSR-2 data land surface temperature on globe.

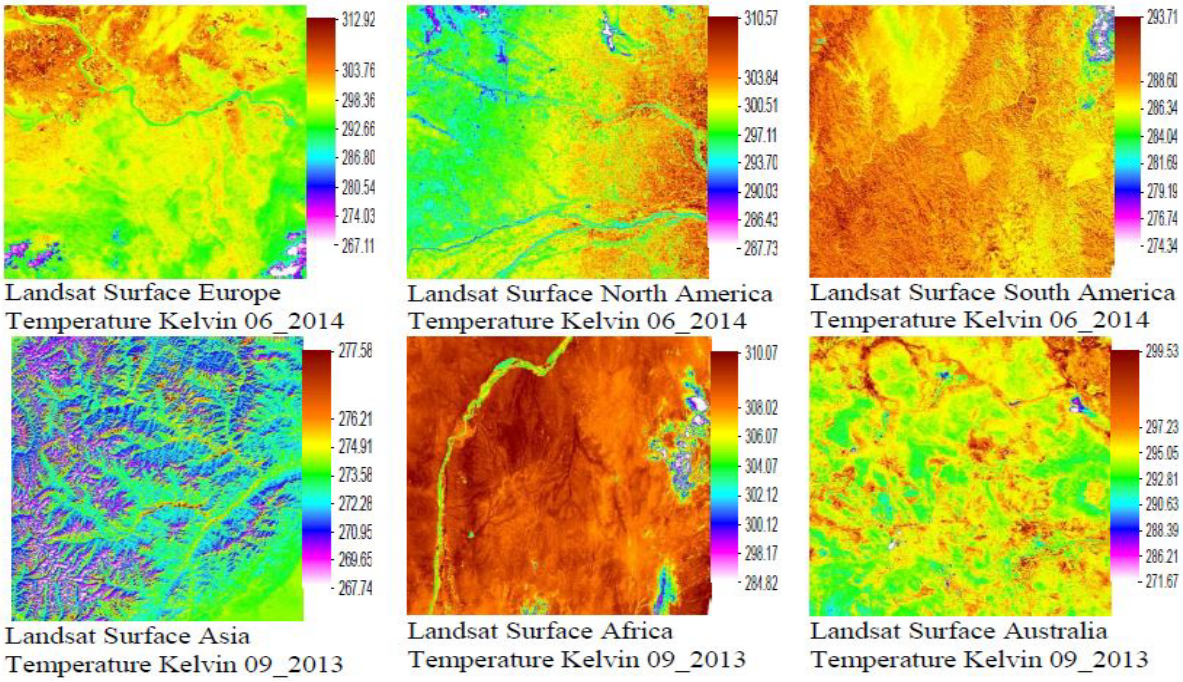

Figure 3: Landsat data land surface temperature on sample site on globe.

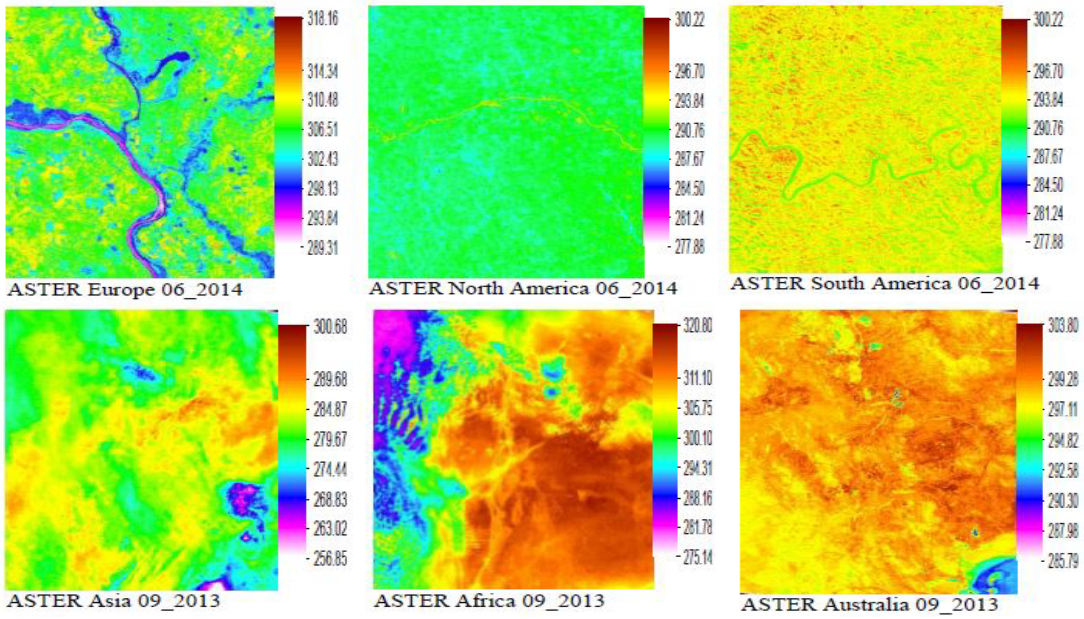

Figure 4: ASTER data land surface temperature on sample site on globe.

Landsat

In 2014 sample site in Europe, Landsat 8 band number 11 shows 267.11 K as lowest temperature and 312.92 K as the highest temperature. Maximum region show around 290 to 300 K temperatures. In North America its 287.73 to 310.57 K and in South America is 274.34 to 293.71 K but maximum region have high temperature, above than 285 K (Figure 3).

In 2013 in Australia the range of temperature is between 271.67 and 299.53 K. For Africa it is 284 to 310 K but a maximum area has above than 305 K temperature, which shows a high temperature. In Asia it's from 267.74 to 277.58 K and maximum area has average temperature (Figure 3).

ASTER

In ASTER data on same location in 2014 in Europe, temperature range is in between 289.31 to 318.16 K and for North America is from 277.88 to 300.22 K. In both regions, maximum area is cool. In South America

and Asia temperature range is 277.88 to 300.22 K and 256.85 to 300.68 K respectively. Maximum area has average temperature. In Africa and Australia it`s 275.14 to 320.80 K and 285.79 to 303.80 K respectively (Figure 4).

Comparing in land surface temperature in AMSR-2, Landsat and ASTER satellite data

In North America Landsat data showing highest and AMSR-2 data is showing lowest temperature in all locations. ASTER data temperature values are in between in North America. In South America ASTER show highest temperature and AMSR-2 lowest and Landsat is in between (Figure 5).

For Europe is same like South America (Table 1). In Africa Landsat have highest and AMSR-2 lowest temperature and ASTER data temperature is in between. In Asia ASTER is highest, than Landsat and

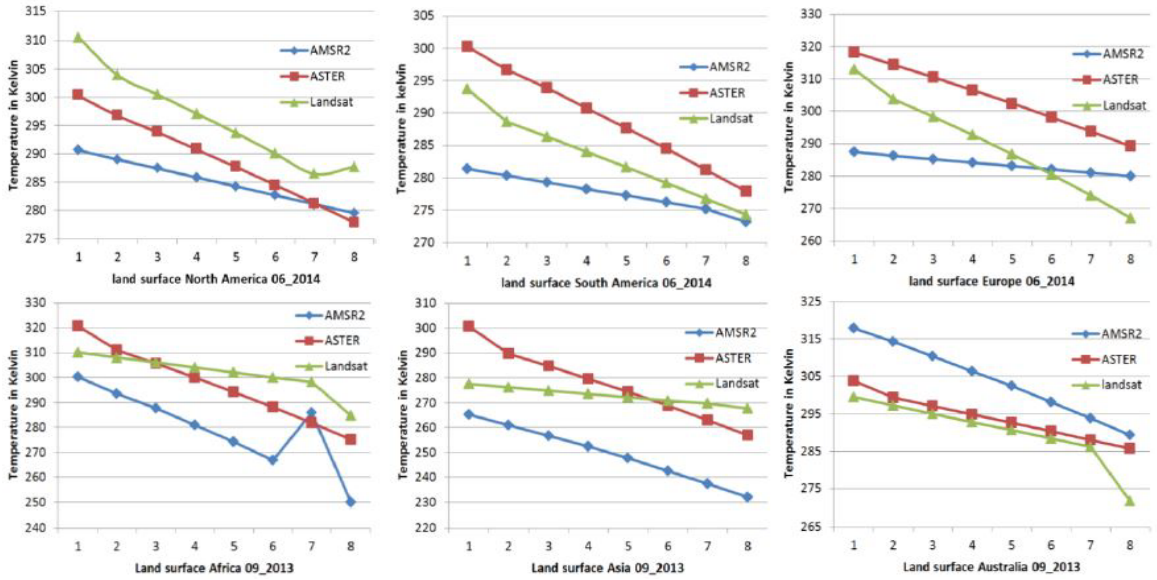

Figure 5: Comparing land surface temperature in ASTER, Landsat and AMSR-2 data.

AMSR2 Tem. K	ASTER Tem. K	Landsat Tem. K
Africa 09_2013		
300.22	320.8	310.07
293.6	311.1	308.02
287.6	305.75	306.07
281.07	300.1	304.07
274.3	294.31	302.12
266.75	288.16	300.12
285.87	281.78	298.17
250.07	275.14	284.42
Asia 09_2013		
265.13	300.68	277.58
260.93	289.68	276.21
256.75	284.47	274.91
252.36	279.67	273.58
247.71	274.44	272.28
242.63	268.83	270.95
237.47	263.02	269.65
232.05	256.85	267.74
Australia 09_2013		
317.96	303.8	299.53
314.34	299.28	297.23
310.48	297.11	295.05
306.44	294.82	292.81
302.43	292.58	290.63
298.13	290.3	288.39
293.76	287.98	286.21
289.31	285.79	271.67

AMSR2 Tem. K	ASTER Tem. K	Landsat Tem. K
North America 06_2014		
290.63	300.22	310.57
288.99	296.7	303.84
287.43	293.84	300.51
285.83	290.76	297.11
284.27	287.67	293.7
282.67	284.5	290.03
281.11	281.24	286.43
279.55	277.88	287.73
South America 06_2014		
281.39	300.22	293.71
280.33	296.7	288.6
279.32	293.84	286.34
278.28	290.76	284.04
277.27	287.67	281.69
276.23	284.5	279.19
275.45	281.24	276.74
273.16	277.28	274.34
Europe 06_2014		
287.44	318.16	312.92
286.33	314.34	303.76
285.27	310.48	298.36
284.19	306.51	292.66
283.14	302.43	286.8
282.06	298.13	280.54
281.01	293.84	274.04
279.95	289.31	267.11

Table 1: Sensor measured temperature in kelvin.

North America	302.10-289.10
South America	293.1-288.10
Europe	303.10-289.10
Asia	300.10-268.10
Africa	311.10-296.10
Australia	302.10-285.10

Table 2: Ground measured temperature in kelvin.

AMSR-2 is the lowest temperature. For Australia, Highest is AMSR-2 than ASTER and Landsat is lowest temperature (Figure 5).

The analysis results show that Landsat and ASTER data temperature is close to ground measurements in compare of AMSR-2 data temperature due to their high resolution and scale (Tables 1 and 2).

Conclusions

Evaluation of different data sources of surface temperature indicates that satellite derived passive microwave surface temperature is not necessarily a superior estimate compared to simulated surface temperature, if evaluated against a data set of observed point measurements. In general, data assimilation systems take into account observational errors and are able, despite errors in the observations, to obtain improvement of land surface temperature results, as long as the temporal trends are well represented. This research work show that Landsat and ASTER is close to ground measurements in compare of AMSR-2 data due to their high resolution and scale.

It should be pointed out that the atmospheric forcing data sets used in the present study are mainly reanalysis data making use of *in-situ* observations. As a consequence, the simulations over the globe with a dense observation network are relatively accurate. However, no or

little observation data are available for all sample sites and the quality of the forcing data and the simulations decreases. Hence, in these areas more scope is present for remote sensing data to constrain this type of research [26,27].

A further consideration is that the retrieval of passive microwave satellite derived surface temperature is hampered by weather conditions: frozen soil conditions in winter and (precipitating) clouds in summer. These phenomena appear to put some emphasis on 'near' in the assessment of the passive microwave retrieval of surface temperature as a 'near all-weather' technique. Consequently, this also applies to the passive microwave soil moisture algorithm retrieval, in case the passive microwave surface temperature estimate is used [28,29].

References

1. Maimaitiyiming M, Ghulm A, Tiyip T, Pla F, Carmona PL, et al. (2014) Effect of green space apatial pattern on the land surface temperature: Implications for sustainable urban planning and climate change adaptation. ISPRS J Photogramm Remote Sens 89: 59-66.
2. Norouzi H, Temimi M, Rossow WB, Pearl C, Azarderakhsh M, et al. (2011) The sensitivity of land emissivity estimates from AMSR-E at C and X bands to surface properties. Hydrol Earth Syst Sci 15: 3577-3589.
3. Boori MS, Netzband M, Vozenilek V, Choudhary K (2015) Urban growth in last three decades in Kuala Lumpur, Malaysia. *IEEE: Joint Urban Remote Sensing Event (JURSE)* 01-04.
4. McCollum JR, Ferraro RR (2005) Microwave rainfall estimation over coasts. J Atmos Ocean Tech 22: 497–512.
5. Min QL, Lin B, Li R (2010) Remote sensing vegetation hydrological states using passive microwave measurements. IEEE Journal of Selected Topics in Applied Earth Observations and Remote Sensing 3: 124–131.
6. Boukabara SA, Weng FZ, Liu QH (2007) Passive microwave remote sensing of extreme weather events using NOAA-18 AMSUA and MHS. IEEE Transactions on Geoscience and Remote Sensing 45: 2228-2246.
7. Entekhabi D, Njoku EG, O'Neill PE, Kellogg KH, Crow WT, et al. (2010) The Soil Moisture Active Passive (SMAP) Mission. Proceedings of the IEEE 98: 704–716.
8. Boori MS, Vozenilek V, Choudhary K (2015) Exposer intensity, vulnerability index and landscape change assessment in Olomouc, Czech Republic. *ISPRS: Int Arch Photogramm Remote Sens Spatial Inf Sci XL-7/W3*: 771 – 776.
9. Zhang LX, Zhao TJ, Jiang LM, Zhao SJ (2010) Estimate of phase transition water content in freeze-thaw process using microwave radiometer. IEEE Transactions on Geoscience and Remote Sensing 48: 4248-4255.
10. Prigent C, Jaumouille E, Chevallier F, Aires F (2008) A parameterization of the microwave land surface emissivity between 19 and 100 GHz, anchored to satellitederived estimates. IEEE Transactions on Geoscience and Remote Sensing 46: 344–352.
11. Norouzi H, Rossow W, Temimi M, Prigent C, Azarderakhsh M, et al. (2012) Using microwave brightness temperature diurnal cycle to improve imissivity retrievals over land. Remote Sensing of Environment 123: 470-442.
12. Boori MS, Vozenilek V, Choudhary K (2015) Land use/cover disturbances due to tourism in Jeseniky Mountain, Czech Republic: A remote sensing and GIS based approach. *The Egyptian Journal of Remote Sensing and Space Sciences* 18: 17 – 26.
13. Njoku EG, Jackson TJ, Lakshmi V, Chan TK, Nghiem SV (2003) Soil moisture retrieval from AMSR-E. IEEE Transactions on Geoscience and Remote Sensing 41: 215–229.
14. Papa F, Prigent C, Rossow WB, Legresy B, Remy F (2006) Inundated wetland dynamics over boreal regions from remote sensing: the use of Topex-Poseidon dual-frequency radar altimeter observations. Int J Remote Sens 27: 4847–4866.
15. Yang H, Yang Z (2006) A modified land surface temperature split window retrieval algorithm and its applications over China. Global and Planetary Change 52: 207-215.
16. Boori MS, Vozenilek V, Choudhary K (2015) Land Use / Cover Change and Vulnerability Evaluation in Olomuc, Czech Republic. ISPRS: Ann Photogramm Remote Sens Spatial Inf Sci II: 77-82.
17. Stephen H, Ahmad S, Piechota TC (2010) Land surface brightness temperature modeling using solar insolation. IEEE Transactions on Geoscience and Remote Sensing 48: 491–498.
18. Aires F, Prigent C, Rossow WB (2004) Temporal interpolation of global surface skin temperature diurnal cycle over land under clear and cloudy conditions. J Geophys Res 109.
19. Chen S, Chen X, Chen W, Su Y, Li D (2011) A simple retrieval method of land surface temperature from AMSR-E passive microwave data – A case study over Southern china during the strong snow disaster of 2008. Int J Appl Earth Obs 13: 140-151.
20. Boori MS, Vozenilek V (2014) Land-cover disturbances due to tourism in Jeseniky mountain region: A remote sensing and GIS based approach. *SPIE Remote Sensing* 9245: 01-11.
21. Fily M, Royer A, Goita K, Prigent C (2003) A simple retrieval method for land surface temperature and fraction of water surface determination from satellite microwave brightness temperatures in sub-arctic areas. Remote Sens Environ 85: 328–338.
22. Karbou F, Gerard E, Rabier F (2006) Microwave land emissivity and skin temperature for AMSU-A and -B assimilation over land. Q J Roy Meteor Soc 132: 2333–2355.
23. Boori MS, Vozenilek V, Burian J (2014) Land-cover disturbances due to tourism in Czech Republic. *Advances in Intelligent Systems and Computing. Springer International Publishing Switzerland* 303: 63-72.
24. Tedesco M, Kim EJ (2006) Retrieval of dry-snow parameters from microwave radiometric data using a dense-medium model and genetic algorithms. IEEE Transactions on Geoscience and Remote Sensing 44: 2143–2151.
25. Wilheit T, Kummerow CD, Ferraro R (2003) Rainfall algorithms for AMSR-E. IEEE Transactions on Geoscience and Remote Sensing 41: 204–214.
26. Boori MS, Ferraro RR (2013) Microwave polarization and gradient ratio (MPGR) for global land surface phenology. J Geol Geosci 2: 01 – 10.
27. Lambin EF, Ehrlich D (1997) Land cover change in sub-saharan Africa (1982-1991): Application of a change index based on remote sensing surface temperature and vegetation indices at a continental scale. Remote Sens Environ 61: 181-200.
28. Prigent C, Rossow WB, Matthews E, Marticorena B (1999) Microwave radiometric signatures of different surface types in deserts. J Geophysl Res Atmos 104: 12147–12158.
29. Boori MS, Amaro VE (2011) A remote sensing and GIS based approach for climate change and adaptation due to sea-level rise and hazards in Apodi-Mossoro estuary, Northeast Brazil. *International Journal of Plant, Animal and Environmental Sciences* 1: 14–25.